Anderson localization of near-visible light in two dimensions

F. Riboli,[1,*] P. Barthelemy,[1] S. Vignolini,[1] F. Intonti,[1] A. De Rossi,[2] S. Combrie,[2] and D. S. Wiersma[1]

[1]*European Laboratory for Non-linear Spectroscopy (LENS) and Consiglio Nazionale delle Ricerche–Istituto Nazionale di Ottica (CNR–INO), I-50019 Sesto Fiorentino (Firenze), Italy*

[2]*THALES Research and Technology, F-91767 Palaiseau Cedex, France*

**Corresponding author: riboli@lens.unifi.it*

Received July 22, 2010; revised October 20, 2010; accepted November 29, 2010; posted December 3, 2010 (Doc. ID 132011); published January 6, 2011

We report on the observation of Anderson localization of near-visible light in two-dimensional systems. Our structures consist of planar waveguides in which disorder is introduced by randomly placing pores with controlled diameter and density. We show how to design structures in which localization can be observed and describe both the realization of the materials and the actual observation of Anderson localized modes by near-field scanning microscopy. © 2011 Optical Society of America

OCIS codes: 160.5298, 180.4243, 260.6042.

Disordered optical materials have fascinating properties owing to the presence of wave interference [1]. An example is their predicted capability to trap optical waves via the optical analogy of an interference phenomenon called Anderson localization. Although originally proposed to describe trapping of electrons in disordered solids [2], Anderson localization has by now been recognized in several types of waves, including sound and matter waves [3,4]. In three dimensions, Anderson localization is a phase transition phenomenon in the disorder parameter [5]. As a result, only very strongly scattering three-dimensional (3D) structures can localize light [3]. In one-dimensional (1D) structures, nearly all states can be Anderson localized, apart from exceptional necklace states in finite size samples. The two-dimensional (2D) case, on the other hand, is critical and constitutes the highest dimension for Gaussian disorder in which no phase transition occurs. So far the effect has been observed in 2D for microwaves[6] and ultrasound [7] but not for near-visible light. The optical wavelength regime is crucial for photonic devices, e.g., devices based on photonic crystals, in which disorder is almost intrinsically present. Understanding and controlling Anderson localization effects in 2D photonic structures is therefore very interesting for creating disorder-based functionalities in photonics [8,9]. Disordered photonic crystals were also used to study an elegant related phenomenon, called transverse localization [10], in which the expansion of a propagating beam is blocked by interference [11].

In this Letter, we report on the observation of Anderson localization in 2D disordered structures for near-visible light, in particular in the telecommunications wavelength range. We explain the considerations for the design of appropriate structures and their realization in planar waveguides. We directly visualize the localized modes with near-field scanning microscopy and show how their characteristics can be tuned by changing the sample parameters. Light waves in our structures are fully confined by the interplay between disorder and in-plane confinement by the waveguide.

The general statement that in 2D all states are localized only holds for ideal random systems of infinite size. In practice, one has to deal with finite size samples and non-zero loss rates, which means that certain conditions need to be fulfilled in order to obtain localized states. First, the localization length must be smaller than the sample size (and smaller than the observation window). Second, the total loss length should be larger than the localization length. While on the one hand one tries to increase the in-plane scattering to minimize the localization length, at the same time one should try to keep the out-of-plane scattering small to minimize losses.

We addressed these design issues with a series of numerical, fully 3D calculations using a commercial finite-difference time-domain (FDTD) code (Crystal Wave by Photon Design, Inc., Oxford, UK). The system consisted of an assembly of randomly placed circular air holes ($n = 1$) in a planar waveguide ($n = 3.5$) of 250 nm core thickness and with an air cladding of 2 μm on both sides, with a 1 μm perfect matching layer surrounding the structure (lateral size $L = 25\ \mu\text{m} \times 25\ \mu\text{m}$, hole diameter hd = 180 – 250 nm, air filling fraction ff = 15–35%). The system was excited by randomly distributed dipole sources at 1.5 μm wavelength, and the resulting signal was recorded by embedding detectors throughout the sample after a variable waiting time.

In Fig. 1(a), we have plotted an example of such a recorded spectrum at various delay times. Also plotted is the total loss rate versus wavelength (dashed red curve). We can see that the spectrum consists of a large number of spikes, which, at longer waiting times, transforms into a much simpler spectrum consisting of a few sharp and isolated peaks located in a window of minimal losses. The spatial distribution of the modes associated with these isolated peaks is localized in a small region of the sample, whose typical size is around $\xi \simeq 2\ \mu\text{m}$ ($\xi \ll L$). In a realistic experiment, one has to target this minimal loss window to be able to observe localized modes. The minimal loss window depends on the pore filling fraction and size and moves to a lower wavelength upon decreasing the pore diameter.

To confirm the localized character of the observed modes, we have calculated the distribution of the intensity normalized to the average intensity $\langle I \rangle$ [Fig. 1(b)]. To that end, we used a system of 20 μm length and 150 μm width and directed a light pulse on its input face. We

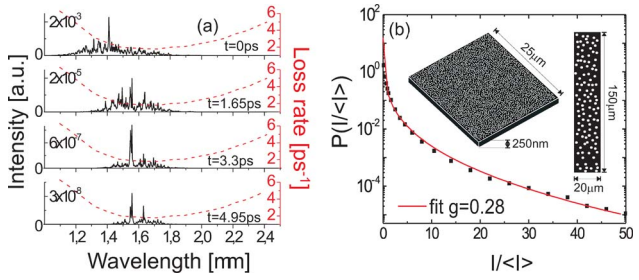

Fig. 1. (Color online) (a) Intensity spectrum inside the structure (ff = 30% and hd = 250 nm) for different waiting times, t, and averaged over position, obtained by Fourier transforming the time evolution of the intensity. (b) Probability distribution of the speckle intensity in transmission (ff = 30% and hd = 250 nm). The two insets show the FDTD layout for the calculation of the intensity spectrum and FWHM (squared layout) and for the calculation of the probability distribution (strip layout).

recorded the time-resolved field on 80 points of the output face and Fourier-transformed this signal to obtain the transmitted speckle intensity. The slowly decaying tail of the intensity distribution is a signature of the occurrence of very strong fluctuations, which are typical for Anderson localization. From the statistics of the intensity speckle it is possible to derive the dimensionless conductance, g, of the system ($g = \delta\omega/\Delta\omega$, with $\delta\omega$ the average spectral width and $\Delta\omega$ the mode spacing). When $g > 1$, the peaks are spectrally overlapping, and thus the system is able to transport light, while for $g < 1$, the modes are localized inside the system [1,12]. The solid curve shows the theoretical curve given by van Rossum and Nieuwenhuizen [12], fitted to our data. This theory [12] has been derived for the mesoscopic regime ($g > 1$). However, experiments with ultrasounds recently demonstrated that its validity extends beyond this mesoscopic regime [13,14]. From this theory we find $g = 0.28$, clearly indicating that the modes are Anderson localized.

Once the system was theoretically characterized, we realized various samples using the appropriate design parameters. These samples were obtained by creating 25 μm × 25 μm broad arrays of air pores, placed at random positions, in a 250-nm-thick planar waveguide of GaAs [15]. A series of samples was made for four hole diameters (180 nm, 200 nm, 220 nm, and 250 nm), and for each hole diameter, samples were made of different filling fractions (20, 25, 30, and 35%).

We created a large number of local sources inside the samples by infiltrating them using two different colloidal solutions of PbS quantum dots (QDs) diluted in toluene, with spectra centered around 1.3 μm [QDs (type I)] or around 1.55 μm [QDs (type 2)] (depending on the spectral region of interest) with a spectral width of 200 nm. The experimental apparatus is built around a commercial scanning near-field optical microscope (SNOM), (TwinSNOM, Omicron NanoTechnology GmbH, Germany). The quantum dots are excited through the SNOM tip with a 780 nm diode laser, and the luminescence signal is collected again through the same tip, fed through a spectrometer and detected by an InGaAs array. This setup has a combined spatial/spectral resolution of 250 nm and 0.5 nm, respectively. We recorded individual emission spectra at 2500 points on each sample. The typical local spectra that we observe (see Fig. 2) contain mostly isolated narrow peaks. In some cases, only one clear peak is observed over the entire wavelength range, whereas in other cases several peaks are found that, however, are nearly always further apart than the spectral width of the individual peaks. This is an important signature of localization, because it means that the Thouless criterion is fulfilled for these modes. Figure 2(d) shows the experimental average FWHM of the observed peaks (assuming a Lorentzian line shape) as a function of the density of holes, for different hole diameters. The experimental values of the FWHM are in good agreement with 3D FDTD calculations performed on the squared layout [inset of Fig. 1(b)]. The average spectral width increases with increasing hole density and hole diameter. Although in this regime of parameters an increased hole diameter would mean an increased scattering strength and hence a reduction of the dimensionless conductance, g, it also means an increase of the out-of-plane losses. In our system, the spectral width of the modes is determined not only by the in-plane conductance (g) but also by the out-of-plane losses. Apparently, this contribution to the width is dominant and explains why increasing the hole diameters increases the modal spectral width.

To gain more insight into the degree of localization of the modes, we have also performed an analysis of their spatial extent. By performing such an analysis, we find that each spectrally isolated peak is associated with a mode strongly localized in space. Figure 3(a) shows the near-field intensity map of such a localized mode, as recorded for Sample 1. The intensity is concentrated in a small region of space, which still covers several scattering elements [see inset of Fig. 3(b)]. This means that the combined trapping due to 2D Anderson localization and total internal reflection in the third direction indeed

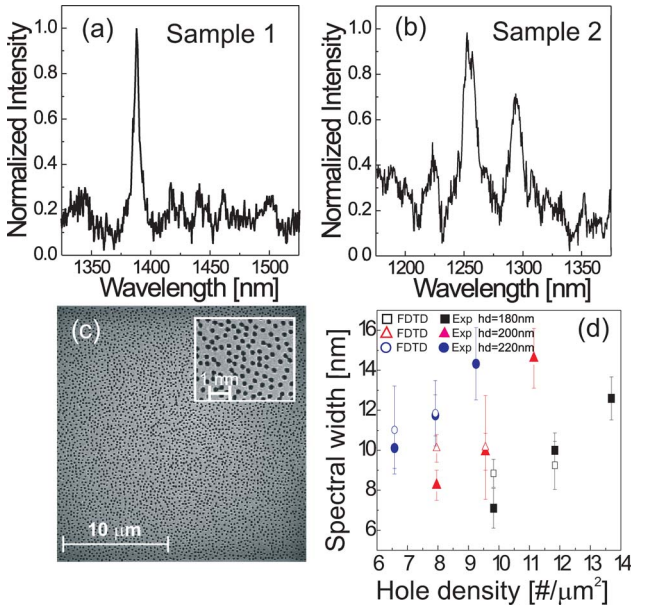

Fig. 2. (Color online) Examples of experimentally observed near-field spectra: (a) ff = 30%, hd = 220 nm; (b) ff = 30% , hd = 250 nm. (c) Scanning electron microscope image of one measured sample. (d) Experimental (filled points) and calculated (empty points) spectral width of the localized modes versus the density of holes.

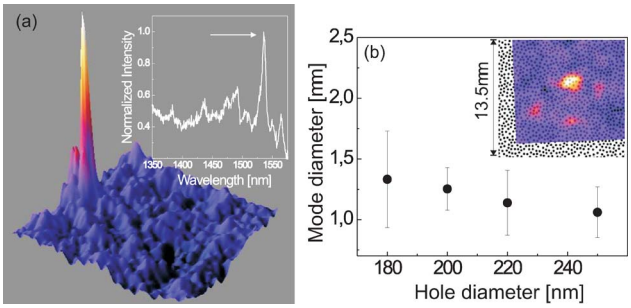

Fig. 3. (Color online) (a) Three-dimensional view of one of the many spatially localized modes as observed in Sample 1. Spatial size image, 13.5 μm × 13.5 μm. The spatial extent of this mode is around 1.4 μm. The inset shows the spectrum recorded in the position where the mode has maximum intensity. (Note: the sample is larger than the scanning area. The actual border is far away from the position of the mode). (b) Average spatial extent of the localized modes as a function of the hole diameter for fixed filling fraction (ff = 0.3). The inset shows the experimental map of one localized mode superimposed to the dielectric matrix of the sample.

makes it possible to confine light to a small spatial region. The inset of Fig. 3(a) shows the normalized intensity spectrum taken at the position corresponding to the maximum of the mode intensity.

From the analysis of the intensity distribution of the localized modes, it is possible to extract information about the spatial extent of such modes as a function of the sample parameters. From this analysis we find a (modest) dependence on scattering strength. To calculate the spatial extent of the modes, we measured the area of each mode within the equi-intensity lines at half-maximum and then calculated the diameter of a disk with equal surface. Figure 3(b) shows the calculated mean spatial diameter of the measured profiles as a function of the hole diameter for a given filling fraction of 30%. Although the overall variation of the mean spatial width is small, the trend seems to be a decrease of the spatial extent as the hole diameter increases.

By combining the results of the spatially resolved and spectrally resolved data and the theory, we obtain a clear picture of the behavior of Anderson localized modes in realistic 2D random structures. It is the interplay among scattering strength, finite sample size, and out-of-plane losses that determines whether localization can be observed and what degree of localization can be achieved. One cannot simply increase the scattering strength at will in the hope of obtaining better confinement, but rather one has to find the right balance among strong scattering, finite-size effects, and intrinsic losses. It is interesting to note that similar considerations hold in the optimization of photonic crystal-based devices and, in particular, photonic crystal cavities, where in-plane confinement should be optimized without increasing the out-of-plane losses. In that case, a small variation in the holes of the photonic crystal around the cavity induces a strong variation in the lifetime of the photonic mode (and hence a large change in spectral width), while the spatial profile is almost conserved.

We wish to thank J. Bertolotti, K. Vynck, and M. Gurioli for fruitful discussions and the use of equipment, and NoE on Nanophotonics for its support. A. De Rossi and S. Combrie acknowledge the support of European Commission (EC) Project GOSPEL (219299).

References

1. P. Sheng, *Introduction to Wave Scattering, Localization and Mesoscopic Phenomena* (Academic, 1996).
2. P. W. Anderson, Phys. Rev. **109**, 1452 (1958).
3. A. Lagendijk, B. van Tiggelen, and D. S. Wiersma, Phys. Today **62**, 24 (2009).
4. A. Aspect and M. Inguscio, Phys. Today **62**, 30 (2009).
5. E. Abrahams, P. W. Anderson, D. C. Licciardello, and T. V. Ramakrishnan, Phys. Rev. Lett. **42**, 673 (1979).
6. D. Laurent, O. Legrand, P. Sebbah, C. Vanneste, and F. Mortessagne, Phys. Rev. Lett. **99**, 253902 (2007).
7. R. L. Weaver, Wave Motion **12**, 129 (1990).
8. J. Topolancik, B. Ilic, and F. Vollmer, Phys. Rev. Lett. **99**, 253901 (2007).
9. L. Sapienza, H. Thyrrestrup, S. Stobble, P. D. Garcia, S. Smolka, and P. Lodahl, Science **327**, 1352 (2010).
10. H. De Raedt, A. Lagendijk, and P. de Vries, Phys. Rev. Lett. **62**, 47 (1989).
11. T. Schwartz, G. Bartal, S. Fishman, and S. Mordechai, Nature **446**, 52 (2007).
12. Th. M. Nieuwenhuizen and M. C. W. van Rossum, Phys. Rev. Lett. **74**, 2674 (1995).
13. H. Hu, A. Strybulevych, J. H. Page, S. E. Skipetrov, and A. Van Tiggelen, Nature Phys. **4**, 945 (2008).
14. A. Z. Genack and J. Wang, Int. J. Mod. Phys. B **24**, 1950 (2010).
15. E. Weidner, S. Combrie, N. Tran, A. De Rossi, J. Nagle, and S. Cassette, Appl. Phys. Lett. **89**, 221104 (2006).